Numerical Solution of the Moment Equations Using Kinetic Flux-Splitting Schemes

Anirudh S. Rana*, Manuel Torrilhon† and Henning Struchtrup*

*Dept. of Mechanical Engineering, University of Victoria, Victoria, BC, Canada
† Center for Computational Engineering Science, Department of Mathematics, RWTH Aachen University, Schinkelstr. 2, D-52062 Aachen, Germany

Abstract. Processes in rarefied gases are accurately described by the Boltzmann equation. The solution of the Boltzmann equation using direct numerical methods and direct simulation Monte Carlo methods (DSMC) is very time consuming. An alternative approach can be obtained by using moment equations, which allow the calculation of processes in the transition regime at reduced computational cost. In the current work, a finite volume method is developed for the solution of these moment equations. The numerical scheme is based on kinetic schemes, similar to those developed for the Euler and Navier-Stokes equations by Deshpande (1986), Perthame (1990), Xu et al. (2005), Le Tallec and Perlat (1998), and others.

Keywords: Boltzmann Equation, Moment Equations, Grad's 13 equations, R13 moment equations, Kinetic flux vector spliting schemes
PACS: 51.10.+y, 47.45.-n, 47.45.Ab, 05.20.Dd

INTRODUCTION

It is well known that the Navier-Stokes and Fourier (NSF) equations of classical hydrodynamics fail to describe non-equilibrium effects in rarefied flows. In a gas, the degree of the rarefaction is defined by the Knudsen number Kn, the ratio of the molecular mean free path (λ) and the geometric characteristic length (L) of the flow.

The Boltzmann equation gives the detailed microscopic description of gas flows at all Knudsen numbers, it describes the evolution of the particle velocity distribution function $f(x_i; t; c_i)$ in phase space. The macroscopic quantities follow from an appropriate integration over the velocity space. In most applications, the solution of the Boltzmann equation using direct numerical methods is rather involved and may lead to serious computational costs. Whereas, the direct simulation Monte Carlo methods (DSMC) [1] method implies stochastic noise, in particular for microflows where the Mach number is very small, making the method computationally expensive.

An alternative approximation can be obtained by moment equations [2], such as, Grad's 13 moment equations [3], Grad's 26 moment equations, Burnett or super-Burnett equations [4], etc. These partial differential equations allow the simulation of the processes at moderate Knudsen numbers in significantly reduced computational time. However, the Burnett and super-Burnett equations are linearly unstable [5] and lack any systematic approach to derive their boundary conditions. On the other hand, the Grad equations are stable but lead to unphysical discontinuous subshocks for large Mach numbers [6].

More recently, Struchtrup & Torrilhon [7] obtained a regularized version of the classical Grad 13-moment equations, known as the R13 equations, by applying a Chapman-Enskog like expansion and order-of-magnitude method to the governing equations of third and higher order moments. This leads to a stable set of 13 governing equations with third order accuracy in the Knudsen number [2], that describe Knudsen layers and produce smooth shock structures for all Mach numbers [8]. The solutions show that the R13 equations can predict all rarefaction effects [9][10], which are observed in solutions of the Boltzmann equation. The R13 equations give quantitatively good agreement to exact data for Knudsen numbers up to Kn $\lesssim 0.35$ [10]. Gu and Emerson [11] have extended the method to 26 moment equations which give reliable results up to Kn $\lesssim 1$.

So far, the R13 system has only been solved for steady state boundary value problems [12, 13] or for time dependent bulk flows [14]. This paper presents a numerical method for non-stationary boundary value problems based on the 2-D unsteady R13 equations. The main focus of this article lies in the interplay between the boundary conditions and the numerical scheme for the linear case. Due to the complexity of the equations and the boundary conditions, the nonlinear case is left for the future.

28th International Symposium on Rarefied Gas Dynamics 2012
AIP Conf. Proc. 1501, 287-293 (2012); doi: 10.1063/1.4769525

R13 EQUATIONS

In kinetic theory macroscopic quantities are associated with the moments of the particle velocity distribution function $f(x_i;t;c_i)$, discribed by the Boltzmann equation. The 13 moment equations are obtained from the Boltzmann equation by multiplying successively by 1, c_i, $c^2/2$, c_ic_j and $c^2c_i/2$, and integrating over velocity space. This procedure gives the mass conservation equation, momentum conservation equation, energy conservation equation, and the balance equations for the pressure tensor and the heat flux vector.

However, moments of higher order always appear in each moment equation and the set of moment equations is not closed, resulting in an infinite set of moment equations. Therefore, a closure procedure is required that relates the higher-order moments, appearing in the flux function of the Boltzmann equation, to those of lower order.

Based upon the Struchtrup and Torrilhon's regularization procedure, one obtains the closed set of R13 equations; here, we give no details but simply present the results of [7]. The linear R13 equations form a system of hyperbolic-parabolic partial differential equations with relaxation, given in their non-dimensionalized formulation, in an 2D orthonormal system as

$$\frac{\partial U}{\partial t} + \text{div}\mathcal{F}(U) - \mathcal{S}(U) = -\text{div}\mathcal{F}^{\nu}(U,\nabla U)\,, \tag{1}$$

where U is a vector of conservative variables, obtained by choosing the first thirteen moments $\Psi(c_i) = \{1, c_i, c^2, c_ic_j - \frac{1}{3}c_kc_k, c^2c_i/2\}$. $\mathcal{F}(U) = [\mathcal{F}_x,\mathcal{F}_y]$ denotes the convective fluxes described by the linearized Grad 13 moment equations, $\mathcal{F}^{\nu}(U,\nabla U) = \left[\mathcal{F}_x^{\nu}, \mathcal{F}_y^{\nu}\right]$ represents the viscous fluxes, and $\mathcal{S}(U)$ is the relaxational source term. In the vector form, U, $\mathcal{F}(U)$, and $\mathcal{S}(U)$ are defined as

$$\begin{aligned}
U &= \left[\rho,\, v_1,\, v_2,\, \frac{3(\theta+\rho)}{2},\, \theta+\rho+\sigma_{11},\, \sigma_{12},\, \theta+\rho+\sigma_{22},\, q_1+\frac{5v_1}{2},\, q_2+\frac{5v_2}{2}\right]^T,\\
\mathcal{F}(U) &= \left[\begin{array}{l} v_1,\, \theta+\rho+\sigma_{11},\sigma_{12},\, q_1+\frac{5v_1}{2},\, \frac{6q_1}{5}+3v_1,\, \frac{2q_2}{5}+v_2,\, \frac{2q_1}{5}+v_1, \\ \qquad\qquad \frac{5}{2}(2\theta+\rho)+\frac{7\sigma_{11}}{2},\, \frac{7\sigma_{12}}{2} \\ v_2,\, \sigma_{12},\, \theta+\rho+\sigma_{22},\, q_2+\frac{5v_2}{2},\, \frac{2q_2}{5}+v_2,\, \frac{2q_1}{5}+v_1,\, \frac{6q_2}{5}+3v_2, \\ \qquad\qquad \frac{7\sigma_{12}}{2},\, \frac{5}{2}(2\theta+\rho)+\frac{7\sigma_{22}}{2} \end{array}\right]^T,\\
\mathcal{F}^{\nu}(U,\nabla U) &= \left[\begin{array}{l} 0,\, 0,\, 0,\, 0,\, m_{111},\, m_{112},\, m_{122},\, \frac{R_{11}}{2},\, \frac{R_{12}}{2} \\ 0,\, 0,\, 0,\, 0,\, m_{112},\, m_{122},\, m_{222},\, \frac{R_{12}}{2},\, \frac{R_{22}}{2} \end{array}\right]^T,\\
\mathcal{S}(U) &= -\frac{1}{\text{Kn}}\left[0,\, 0,\, 0,\, 0,\, \sigma_{11},\, \sigma_{12},\, \sigma_{22},\, \frac{2q_1}{3},\, \frac{2q_2}{3}\right]^T,
\end{aligned}$$

where ρ is the gas density, θ is the temperature in energy units, v_i is the flow velocity, q_i is the heat flux vector, σ_{ij} is the stress tensor, and Kn is the corresponding Knudsen number. Here, m_{ijk} and R_{ij} represent higher moments and, as such, contribute to the fluxes of stress and heat flux. The R13 theory provides the gradient expressions for these quantities as [7]

$$\begin{aligned}
m_{111} &= -2\text{Kn}\left(\tfrac{3}{5}\tfrac{\partial\sigma_{11}}{\partial x} - \tfrac{2}{5}\tfrac{\partial\sigma_{12}}{\partial y}\right), & m_{112} &= -2\text{Kn}\left(\tfrac{8}{15}\tfrac{\partial\sigma_{12}}{\partial x} + \tfrac{1}{3}\tfrac{\partial\sigma_{11}}{\partial y} - \tfrac{2}{15}\tfrac{\partial\sigma_{22}}{\partial y}\right),\\
m_{122} &= -2\text{Kn}\left(\tfrac{8}{15}\tfrac{\partial\sigma_{12}}{\partial y} + \tfrac{1}{3}\tfrac{\partial\sigma_{22}}{\partial x} - \tfrac{2}{15}\tfrac{\partial\sigma_{11}}{\partial x}\right), & m_{222} &= -2\text{Kn}\left(\tfrac{3}{5}\tfrac{\partial\sigma_{22}}{\partial y} - \tfrac{2}{5}\tfrac{\partial\sigma_{12}}{\partial x}\right),
\end{aligned} \tag{2}$$

and

$$R_{11} = -4\text{Kn}\left(\frac{9}{5}\frac{\partial q_1}{\partial x} + \frac{3}{5}\frac{\partial q_2}{\partial y}\right), R_{12} = -\frac{12}{5}\text{Kn}\left(\frac{\partial q_2}{\partial x} + \frac{\partial q_1}{\partial y}\right), R_{22} = -4\text{Kn}\left(\frac{3}{5}\frac{\partial q_1}{\partial x} + \frac{9}{5}\frac{\partial q_2}{\partial y}\right). \tag{3}$$

Note that for $m_{ijk} = 0$ and $R_{ij} = 0$ the R13 equations reduce to Grad's original 13-moment system [3].

NUMERICAL SCHEME

In order to formulate a finite volume scheme for the linerized R13 equations, we first discretize the computational domain with constant spatial rectangular cells, Ω_{ij}, of size Δx and Δy in the x and y directions, respectively. By

integrating Eq. (1) over each cell Ω_{ij}, and using the Gauss divergence theorem on the surface integral we obtain a set of semi-discrete ordinary differential equations,

$$\frac{d\overline{U}_{ij}}{dt} + \frac{1}{\Delta x}\left(\mathcal{F}_x^{i+1/2,j} - \mathcal{F}_x^{i-1/2,j}\right) + \frac{1}{\Delta y}\left(\mathcal{F}_y^{i,j+1/2} - \mathcal{F}_y^{i,j-1/2}\right) - S\left(\overline{U}_{ij}\right)$$
$$= -\frac{1}{\Delta x}\left(\mathcal{F}_x^{\nu\, i+1/2,j} - \mathcal{F}_x^{\nu\, i-1/2,j}\right) - \frac{1}{\Delta y}\left(\mathcal{F}_y^{\nu\, i,j+1/2} - \mathcal{F}_y^{\nu i,j-1/2}\right). \tag{4}$$

Here, $\overline{U}_{ij} = \iint_{\Omega_{ij}} U dxdy$ is the cell average value of U.

Due to the discontinuous function approximation, flux terms in Eq. (4), i.e., $\mathcal{F}_x^{i\pm1/2,j}$, $\mathcal{F}_x^{\nu\, i\pm1/2,j}$, $\mathcal{F}_y^{i,j\pm1/2}$ and $\mathcal{F}_y^{\nu\, i,j\pm1/2}$ are not uniquely defined at cell interfaces. The flux functions $\mathcal{F}$ appearing in the last equations are in fact replaced by a numerical flux function $\mathcal{F}_x^{i\pm1/2,j} = F_x^N\left(\overline{U}_{ij}^{(+)}, \overline{U}_{i\pm1,j}^{(-)}\right)$ which depends on the internal interface values $\overline{U}_{ij}^{(+)}$, and on the neighboring element interface values $\overline{U}_{i\pm1,j}^{(-)}$.

For a first-order scheme, the cell interface values $\overline{U}_{ij}^{(+)}$ and $\overline{U}_{i+1\,j}^{(-)}$ are simply taken as the cell average value of $\overline{U}_{ij}$ corresponding to the control volume on either side of the face. To obtain second-order accuracy in space, we used a linear reconstruction of the cell interface values $\overline{U}_{ij}^{(+)}$ and $\overline{U}_{i+1\,j}^{(-)}$, defined as

$$\overline{U}_{ij}^{(+)} = \left(\frac{4\overline{U}_{ij} + \overline{U}_{i+1,j} - \overline{U}_{i-1,j}}{4}\right), \overline{U}_{i+1,j}^{(-)} = \left(\frac{4\overline{U}_{i+1,j} - \overline{U}_{i+2,j} + \overline{U}_{ij}}{4}\right). \tag{5}$$

Another possibility instead of using Eq. (5) is to introduce limiters such as the minmod or superbee [19]; however, due to the fact that we concentrate on shockless problems, we did not find it necessary to introduce any kind of limiting procedure.

Different choices for these numerical fluxes give rise to different finite volume schemes [19]. For the hyperbolic part, a few of these numerical schemes are briefly presented in the next subsection.

Discretization of Inviscid Fluxes

In general the approximate numerical fluxes at each cell face can be written as

$$F^N\left(\overline{U}_{ij}^{(+)}, \overline{U}_{i+1,j}^{(-)}\right) = \frac{\mathcal{F}\left(\overline{U}_{ij}^{(+)}\right) + \mathcal{F}\left(\overline{U}_{i+1,j}^{(-)}\right)}{2} - \frac{1}{2}\mathcal{D}\left(\overline{U}_{i+1,j}^{(-)} - \overline{U}_{ij}^{(+)}\right). \tag{6}$$

where $\mathcal{F}(U)$ represents the convective flux and $\mathcal{D}$ denotes the diffusion matrix.

In the Roe scheme the diffusion matrix $\mathcal{D}$ is given by $T|\Lambda|T^{-1}$. Here, Λ is the diagonal matrix consisting of the eigenvalues of the Jacobian of the flux $\mathcal{F}_x$ and T is the matrix of corresponding eigenvectors. Similarly, in the Rusanov scheme $\mathcal{D} = |\lambda_{\max}|I$, where the diffusion operator for a system is simply approximated by the largest signal speed $\lambda_{\max}$ [19].

The Rusanov scheme is attractive because of its simplicity and robustness, however, it loses detail due to larger numerical diffusion [19]. On the other hand, the Roe scheme is more accurate, but it requires a full eigenvalue decomposition of the flux Jacobian.

Usually, for a large non-linear system, such as Grad 13 or Grad 26, an eigenvalue decomposition of the Jacobian matrix is not known a priory, therefore, constructing a Roe scheme would be very complicated and computationally expensive. The Kinetic Flux Vector Splitting (KFVS) schemes [20] are an interesting alternative to the traditional approaches and provide basically the same advantages as that of the upwind scheme, without requiring any eigenvalue decomposition.

In KFVS schemes, we start with the 2-D Boltzmann equation without the collision term and develop an upwind scheme at the microscopic level as

$$\frac{\partial f}{\partial t}+\frac{c_k+|c_k|}{2}\frac{\partial f}{\partial x_k}+\frac{c_k-|c_k|}{2}\frac{\partial f}{\partial x_k}=0,$$

where c_k are the microscopic velocities.The numerical fluxes across the cell interface are now constructed by taking suitable moments, which after some simplification read

$$F_x^{Kin}\left(\overline{U}_{ij}^{(+)},\overline{U}_{i+1,j}^{(-)}\right)=\int_{c_1\geq 0}\psi c_1 f\left(\overline{U}_{ij}^{(+)},c_k\right)dc+\int_{c_1\leq 0}\psi c_1 f\left(\overline{U}_{i+1,\,j}^{(-)},c_k\right)dc, \tag{7}$$

and

$$F_y^{Kin}\left(\overline{U}_{ij}^{(+)},\overline{U}_{i,j+1}^{(-)}\right)=\int_{c_2\geq 0}\psi c_2 f\left(\overline{U}_{ij}^{(+)},c_k\right)dc+\int_{c_2\leq 0}\psi c_2 f\left(\overline{U}_{i,j+1}^{(-)},c_k\right)dc. \tag{8}$$

Any distribution function, f which reproduces the moment equations can be used in Eqs. (7-8) but for computational efficiency, we desire that the distribution function should allow an explicit evaluation of the half space integrals in Eqs. (7-8), therefore, we choose the linearized Grad 13 distribution function

$$f_{|13}=\frac{\rho}{\sqrt{2\pi\theta}^3}\exp\left(-\frac{c^2}{2\theta}\right)\left[1+\frac{c_i v_i}{\theta}+\frac{\sigma_{ij}}{2\rho\theta^2}c_{\langle i}c_{j\rangle}+\frac{1}{5}\frac{q_i}{\rho\theta^2}c_i\left(\frac{c^2}{\theta}-5\right)\right]$$

where c_i are the microscopic velocities.

Discretization of Diffusive Fluxes

Evaluation of the viscous fluxes requires the discretization of spatial derivatives at the cell interfaces. We discretize x and y derivatives by using the second order central difference method, for example, at the interface between the Ω_{ij} and $\Omega_{i+1,j}$ cells, we approximate the derivative of some quantity, g as

$$\frac{\partial g}{\partial x}|_{i+1/2,j}=\frac{g_{i+1,j}-g_{ij}}{\Delta x}\text{ and }\frac{\partial g}{\partial y}|_{i+1/2,j}=\frac{6\left(g_{i,j+1}-g_{i,j-1}\right)+3\left(g_{i+1,\,j+1}-g_{i+1,\,j-1}\right)-\left(g_{i-1,\,j+1}-g_{i-1,\,j-1}\right)}{16\Delta y}. \tag{9}$$

Implementation of the Boundary Conditions

A derivation and discussion of the surface boundary conditions for the R13 system is given in [16]. To explain the implementation of these boundary conditions, let us consider a surface where the wall normal is along the y direction. The boundary conditions follow from Maxwell's accommodation model [16]

$$v_2=0 \tag{10a}$$

$$\sigma_{12}=\frac{-\chi}{2-\chi}\sqrt{\frac{2}{\pi}}\left(\mathcal{V}_1+\frac{1}{5}q_1+\frac{1}{2}m_{122}\right), \tag{10b}$$

$$q_2=\frac{-\chi}{2-\chi}\sqrt{\frac{2}{\pi}}\left(2\mathcal{T}+\frac{1}{2}\theta\sigma_{22}+\frac{1}{112}R_{11}+\frac{3}{16}R_{22}\right), \tag{10c}$$

$$R_{12}=\frac{\chi}{2-\chi}\sqrt{\frac{2}{\pi}}\left(\mathcal{V}_1-\frac{11}{5}q_1-\frac{1}{2}m_{122}\right), \tag{10d}$$

$$m_{222}=\frac{\chi}{2-\chi}\sqrt{\frac{2}{\pi}}\left(\frac{2}{5}\mathcal{T}-\frac{7}{5}\sigma_{22}+\frac{13}{280}R_{11}-\frac{1}{40}R_{22}\right), \tag{10e}$$

$$m_{112}=\frac{-\chi}{2-\chi}\sqrt{\frac{2}{\pi}}\left(\frac{1}{5}\mathcal{T}+\frac{1}{20}R_{11}+\sigma_{11}-\frac{1}{5}\sigma_{22}-\frac{3}{140}R_{22}\right), \tag{10f}$$

where $\mathcal{V}_1 = v_1 - v_1^W$ and $\mathcal{T} = \theta - \theta_W$ are the slip velocity and temperature jump, respectively, and χ is the accommodation coefficient. The higher order moments, i.e. m_{ijk} and R_{ij}, appearing in the boundary conditions are related to the field variables, $\{\rho, v_i, T, \sigma_{ij}, q_i\}$, by the R13 constitutive relations given in Eqs. (2)–(3). Due to rotational symmetry, analogous expressions can be obtained for the x direction as well.

In the convective fluxes on the boundary, odd fluxes in normal direction (i.e. v_2, σ_{12}, and q_2 for the y direction), are replaced with the boundary conditions Eqs. (10a)–(10c). Whereas, even quantities, such as v_1, q_1, σ_{11}, σ_{22}, or θ, are determined from inner nodes using a second order extrapolation. Similarly, for the diffusive fluxes on the boundary, odd fluxes, such as m_{112}, m_{222}, and R_{12} for the y direction are replaced by the boundary conditions (10d)–(10f), whereas even fluxes, such as m_{111}, m_{122}, R_{11}, and R_{22}, are determined from the inner nodes using a second order extrapolation.

Time Integration

For time integration, we used a second order, stiffly accurate IMEX-SSP2(2,2,2) scheme based on an explicit and implicit tableau [21]

$$\begin{array}{cc} 0 & 0 \\ 1 & 0 \\ \hline \frac{1}{2} & \frac{1}{2} \end{array} \quad \text{and} \quad \begin{array}{cc} \gamma & 0 \\ 1-2\gamma & \gamma \\ \hline \frac{1}{2} & \frac{1}{2} \end{array}$$

where, $\gamma = 1 - 1/\sqrt{2}$. This scheme gives a stability constraint $\Delta t \leq \frac{1}{2} \min\left(\frac{\Delta x^2}{|a_{\max}|\Delta x + 2\mu}, \frac{\Delta y^2}{|a_{\max}|\Delta y + 2\mu}\right)$, where $a_{\max} = 2.13$ is the maximal eigenvalue for the Grad13 system and μ is the coefficient of viscosity.

NUMERICAL EXPERIMENTS

Convergence Test

For a demonstration of the convergence properties for this numerical scheme we obtain a numerical solution for 1-dimensional Poiseuille flow and compare it against the exact solution for the steady state obtained analytically, which can be found in [9]. A graphical comparison between the Roe, Rusanov and the KFVS schemes is shown in figure 1, where the error (in L_1-norm) is plotted on a logarithmic scale against the number of cells. For these numerical computations, the initial condition is chosen as the steady state solution obtained analytically in [9]. Each subplot in

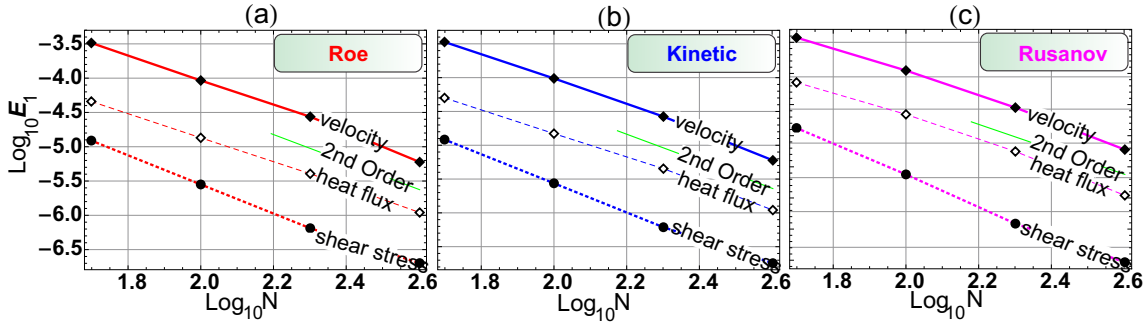

FIGURE 1. Figures (a), (b), and (c) illustrate the log-log plots of the error vs. the number of grid-cells for the numerical solution of the R13 system, simulated using the Roe scheme, KFVS scheme, and Rusonov scheme, respectively.

figure 1 shows the error of velocity, as continuous lines, heat flux, indicated by dashed lines, and shear stress, as dotted lines. Here it is clearly visible that the numerical solution converges at approximately 2nd order.

Oscillatory Heating

As an example for a 2-D transient process, we study the following problem: Let us consider a monoatomic gas confined inside a square enclosure of width L. The plate at $y = 0$ is heated with an oscillatory wall temperature, $\theta_W = \theta_0 + \Delta\theta \cos(\omega t)$, while the temperature of the other plates are kept at an ambient temperature θ_0.

Analysis of this process requires consideration of rarefaction and non-stationary effects, which are characterized by the Knudsen number (based on width L of the enclosure) and dimensionless oscillating frequency (ω), respectively. For the computations in this paper, we consider $\omega = 1$ and $\Delta\theta = 0.1\theta_0$.

Figure 2 illustrates the variation of the net dimensionless heat transfer from the bottom surface, defined as

$$Q = \frac{\theta_0}{\Delta\theta} \int_0^1 \hat{q}_y(\hat{x}, 0)\, d\hat{x}\,, \tag{11}$$

over a period of time $\hat{t} = t\sqrt{\theta}/L$. Results obtained by solving R13 (continuous, red), Grad 13 (dashed, blue), and NSF with first order (thin, green) boundary conditions are presented in figure 2 for three different Knudsen numbers. As we see from figure 2, with increasing Knudsen number the amplitude of Q increases since temperature gradients inside the cavity become steeper. At the relatively small Knudsen number of 0.05, R13, Grad 13, and NSF show good

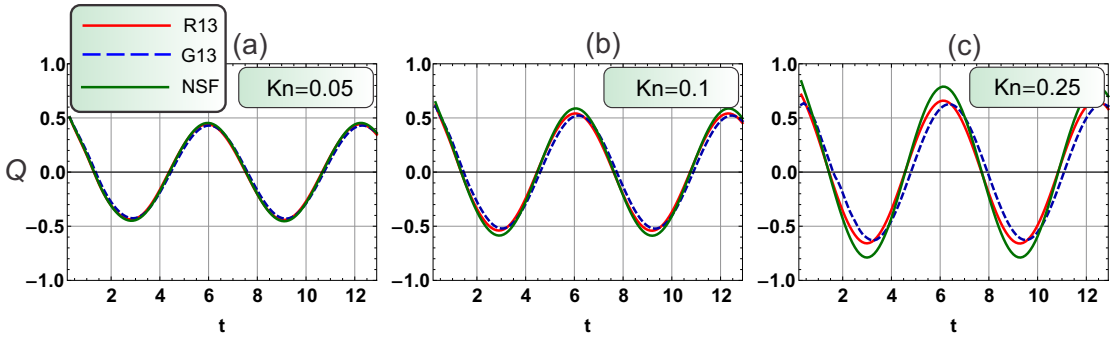

FIGURE 2. Time evolution of the net dimensionless heat flux from the bottom plate, obtained by solving R13(continuous,red), NSF with first order boundary conditions (thin, green) and Grad 13 (dashed, blue) for Kn = 0.05, 0.1, and 0.25.

agreement ($\lessapprox 2\%$ deviation in amplitude). For larger Knudsen numbers, where rarefaction effects are prominent, NSF overestimates the net heat transfer with approximately 20% deviation in the magnitude. This result is consistent with the computation performed under the steady state assumption [13].

Figure 3 shows the amplitude of dimensionless temperature for the R13 equations for three different Knudsen numbers. As the Knudsen number increases, the amplitude decreases due to increasing temperature jump. Figure 4 shows the dimensionless density amplitude. It follows that as temperature amplitude decreases, density amplitude decreases as well.

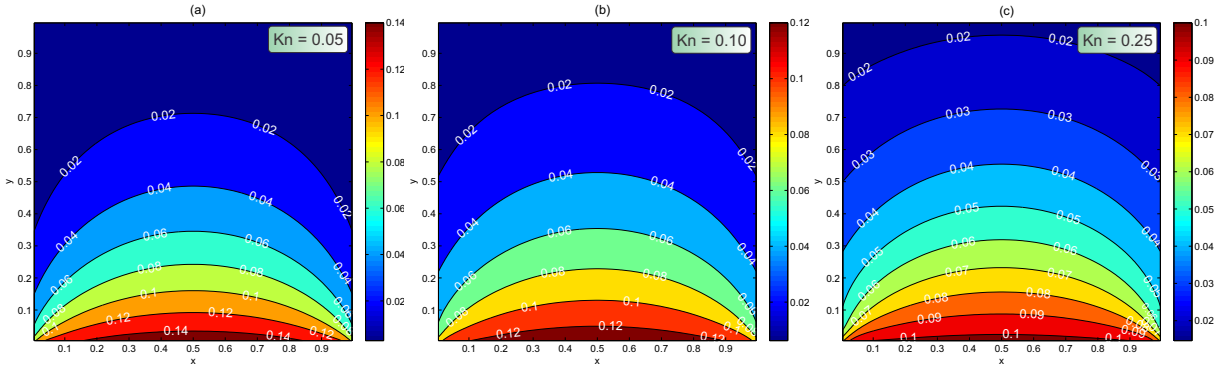

FIGURE 3. Amplitude of the dimensionless temperature, for Kn = 0.05, 0.1, and 0.25.

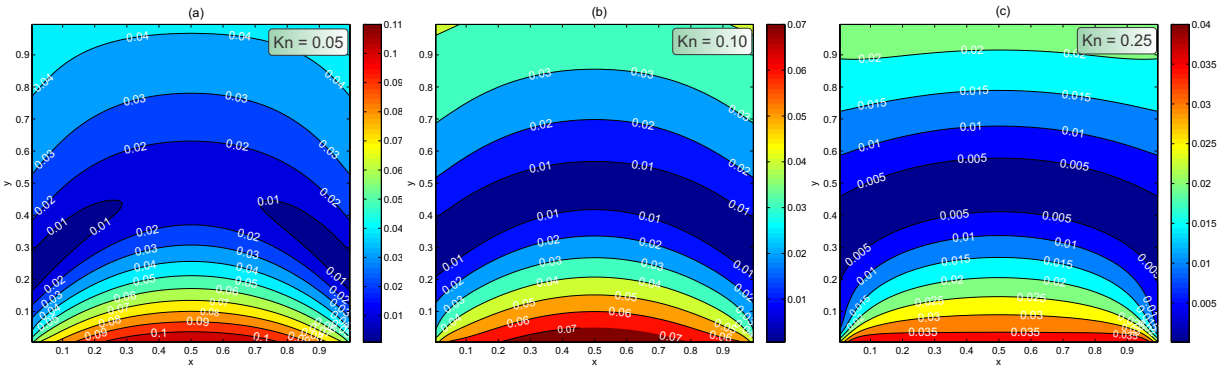

FIGURE 4. Amplitude of the dimensionless density, for Kn = 0.05, 0.1, and 0.25.

CONCLUSIONS

The non-stationary boundary value problems has been solved numerically by using a finite volume method based on the kinetic flux vector splitting (KFVS) scheme. The KFVS scheme has an advantage over the Roe scheme as it does not require any eigenvalue decomposition of the flux Jacobian, which will be useful for solving larger non-linear systems, such as higher moment equations.

In particular we solved the oscillatory heat flow problem for a rarefied gas contained inside a square enclosure using linearized moment equations, NSF with first order slip and jump boundary conditions, the Grad 13 equations and the R13 equations. We found that the amplitude of the net heat from the heated surface, Q increases as Knudsen number increases from the hydrodynamic regime to the transition flow regime. Moreover, NSF overestimates the net heat transfer for larger Knudsen numbers. Future work would include extending this numerical scheme to non-linear R13 system.

REFERENCES

1. G. A. Bird, *Molecular Gas Dynamics and the Direct Simulation of Gas Flows*, Oxford University Press, Oxford (1994).
2. H. Struchtrup, *Macroscopic Transport Equations for Rarefied Gas Flows*, Springer, New York (2005).
3. H. Grad, *Comm. Pure Appl. Math.* **2**, 331-407 (1949).
4. D. Burnett, *Proc. Lond. Math. Soc.* **40**, 382-435 (1936).
5. A.V. Bobylev, *J. Stat. Phys.* **124**, 371-399 (2006).
6. I. Muller, T. Ruggeri, *Rational Extended Thermodynamics*, Springer, 2nd edition (1998).
7. H. Struchtrup and M. Torrilhon, *Phys. Fluids* **15**, 2668-2680 (2003).
8. M. Torrilhon and H. Struchtrup, *J. Fluid Mech.* **513**, 171-198 (2004).
9. P. Taheri, M. Torrilhon, and H. Struchtrup, *Phys. Fluids* **21**, 017102 (2009).
10. P. Taheri, A. S. Rana, M. Torrilhon and H. Struchtrup, *Continuum Mech. Thermodyn.* **21**, 423–443 (2009).
11. X. J. Gu and D. R. Emerson, *J. Fluid Mech.* **636**, 177–216 (2009).
12. H. Struchtrup and M. Torrilhon, *Phys. Rev. E* **78**, 046301 (2008).
13. A. S. Rana, M. Torrilhon and H. Struchtrup, *J. Phys.: Conf. Ser.* **362**, 012034 (2012).
14. M. Torrilhon, *SIAM Multiscale Model. Simul.* **5**, 695–728 (2006).
15. H. Struchtrup and M. Torrilhon, *Phys. Rev. Lett.* **99**, 014502 (2007)
16. M. Torrilhon and H. Struchtrup, *J. Comp. Phys.* **227**, 1982-2011 (2008).
17. P. Taheri and H. Struchtrup, *Int. J. Heat Mass Tran.* **55**, 1291–1303 (2012)
18. H. Struchtrup, *J. Stat. Phys.* **125**, 565-587 (2006).
19. R. J. LeVeque, *Finite Volume Methods for Hyperbolic Problems*, Cambridge University Press, Cambridge, UK (2002).
20. S.M. Deshpande, *AIAA Aerospace Sciences Meeting, 24th, Reno, NV* (1986).
21. L. Pareschi and G. Russo, *J. Sci. Comput.* **25**, 129-155 (2004).